Published in final edited form as:
Annu Rev Fluid Mech. 2009 January 1; 41: 91–107. doi:10.1146/annurev.fluid.40.111406.102126.

Hemodynamics of Cerebral Aneurysms

Daniel M. Sforza[1], **Christopher M. Putman**[2,3], and **Juan Raul Cebral**[1]
Daniel M. Sforza: ; Christopher M. Putman: ; Juan Raul Cebral: jcebral@gmu.edu
[1]Center for Computational Fluid Dynamics, George Mason University, Fairfax, Virginia 22030
[2]Interventional Neuroradiology, Inova Fairfax Hospital, Falls Church, Virginia 22042
[3]Department of Neurosurgery, School of Medicine, George Washington University, Washington, DC 20037

Abstract

The initiation and progression of cerebral aneurysms are degenerative processes of the arterial wall driven by a complex interaction of biological and hemodynamic factors. Endothelial cells on the artery wall respond physiologically to blood-flow patterns. In normal conditions, these responses are associated with nonpathological tissue remodeling and adaptation. The combination of abnormal blood patterns and genetics predisposition could lead to the pathological formation of aneurysms. Here, we review recent progress on the basic mechanisms of aneurysm formation and evolution, with a focus on the role of hemodynamic patterns.

Keywords

intracranial aneurysms; computational fluid dynamics; wall shear stress; growth; rupture

1. Introduction

Cerebral aneurysms are pathological dilatations of the arterial walls frequently located near arterial bifurcations in the circle of Willis (Stehbens 1972, Weir 2002, Wiebers et al. 2004). Their most serious consequences are their rupture and intracranial hemorrhage, with an associated high mortality and morbidity rate (Kaminogo et al. 2003, Linn et al. 1996, Winn et al. 2002). Intracranial aneurysms are particularly difficult to treat and often do not produce symptoms before they rupture. Improvement of neuroradiological techniques has resulted in more frequent detection of unruptured aneurysms. Because prognosis of subarachnoid hemorrhage is still poor, preventive surgery is increasingly considered as a therapeutic option. However, every treatment carries a risk, which sometimes matches or exceeds the yearly risk of aneurysm rupture. Therefore, the best patient care would be to treat only those aneurysms that are likely to rupture (Kassell et al. 1990). Planning elective surgery requires a better understanding of the process of aneurysm formation, progression, and rupture so that one can make a sound judgment of the risks and benefits of possible therapies. Unfortunately, these processes are not well understood. Previous studies (Boecher-Schwarz et al. 2000, Buonocore 1998, Gobin et al. 1994, Groden et al. 2001, Kayembe et al. 1984, Kerber & Heilman 1983, Kerber et al. 1999, Kyriacou & Humphrey 1996, Metcalfe 2003, Ortega 1998, Stehbens 1972) have identified the major factors involved in these processes: (*a*) hemodynamics, (*b*) wall biomechanics, (*c*) mechanobiology, and (*d*) the intracranial environment. In the following sections, we review these factors and, in particular, concentrate on the role of hemodynamics.

2. Mechanisms of Aneurysm Growth and Rupture

Central to any hypothesis of the pathogenesis of aneurysm growth and rupture is the interaction between the hemodynamic forces and the vessel wall biology and the resulting impact on the wall's mechanics. Ultimately, any rupture is the consequence of the inability of the wall to contain the force of the flowing blood. Yet hemodynamic studies have not found evidence of excessive elevations of peak pressure within cerebral aneurysms to explain the wall failure on a purely mechanical basis. Consequently, there must be an alteration of the aneurysmal wall that results in its mechanical weakening over time.

2.1. Histological Observations

Histological studies have found a decreased number (or the degeneration of) endothelial cells, the degeneration of the internal elastic lamina, and thinning of the medial layer (Stehbens 1963, Stehbens 1989). Because the internal elastic lamina and vascular extracellular matrix are considered the main contributors to the structural integrity of the vessel, investigators have examined a variety of enzymes related to their remodeling and potential degeneration. Circulating levels of serum gelatinase or elastase are increased in patients with cerebral aneurysms (Chyatte & Lewis 1997). Increased matrix metalloproteinase has been found in aneurysm walls (Bruno et al. 1998). These enzymes are largely responsible for intracellular matrix degradation as part of the process of wall remodeling; therefore, increased activity could cause weakening of the wall. Thinning of the medial layer in the aneurysm wall seen histologically has been largely explained by a decreased number of smooth muscle cells (Kondo et al. 1998; Stehbens 1963, 1989). Both experimental and clinical studies have attributed the decrease of smooth muscle cells to their apoptosis (Hara et al. 1998, Kondo et al. 1998). Consequently, it is widely believed that smooth muscle–cell apoptosis and elastin/collagen fiber–reconstitution mechanisms are central to the process of wall weakening.

2.2. Genetic Factors

The interplay of genetics and biomechanical stimuli generated by blood flow seems to be a critical element in the pathogenesis of cerebral aneurysms. Animal studies have pointed to endothelial degeneration and cell loss as the initiating event of aneurysm wall remodeling (Kojima et al. 1986). Furthermore, a study on Japanese patients found a genetic locus for cerebral aneurysms localized within or close to the elastin gene locus on chromosome 7 (Onda et al. 2001). Endothelial gene expression is related to wall shear stress (WSS). Prolonged laminar WSS regulates expression to only a small percentage (1%–5%) of endothelial genes, and this transcriptional profile produces an endothelial phenotype that is quiescent, protected from apoptosis, inflammation, and oxidative stress (Wasserman 2004). Therefore, triggering for genetic traits, potentially affecting arterial wall mechanical-load tolerance, may be attributed to a hemodynamic condition.

2.3. Hemodynamic Factors

The capacity of the endothelial cell to sense WSS is an important determinant of lumen diameter and overall vessel structural remodeling (Drexler & Hornig 1999, Luscher & Tanner 1993). This morphological variation of the vascular endothelium layer results in different production levels of vasoactive substances such as nitric oxide (NO) (Guzman et al. 1997, Kamiya et al. 1988, Luscher & Tanner 1993). Studies indicate that low wall stress and high oscillatory patterns of WSS cause intimal wall thickening (Dardik et al. 2005, Friedman et al. 1981, Ku et al. 1985). A uniform shear stress field tends to stretch and align the endothelial cells in the direction of the flow, whereas low–shear stress levels in an oscillatory hemodynamic environment cause irregular shape and the loss of a particular orientation. Furthermore, low WSS was found to switch the endothelial cell phenotype from atheroprotective to atherogenic

with a high endothelial cell turnover rate (Ford et al. 2005a). This could be protective for aneurysms because the wall tends to thicken.

In summary, the caliber and also the histological structure of arterial walls are regulated by blood flow, particularly by WSS. In the presence of endothelial cells and smooth muscle cells, a chronic increase of WSS due to increased arterial blood flow elicits an adaptive response of the arterial wall histology, leading to vessel enlargement and a reduction in WSS to physiological baseline values. However, if WSS is increased focally, it can potentially cause a focal enlargement of and damage to the arterial wall, termed destructive remodeling, which is induced by the excessive production of molecules such as NO.

2.4. Aneurysm Initiation

The formation of cerebral aneurysms is believed to be related to an interaction between high-flow hemodynamic forces and the arterial wall owing to several clinical and experimental observations. Cerebral aneurysms are commonly associated with anatomic variations and pathological conditions (such as hypoplasia or occlusion of a segment of the circle of Willis) (Kayembe et al. 1984; Matsuda et al. 1983; Salar & Mingrino 1977, 1981; Yasargil 1984), or high-flow arteriovenous malformations that cause locally increased flow in the cerebral circulation (Peerless & Drake 1982), and, at points of flow bifurcation, a site of flow separation and elevated WSS. Observations from animal models have shown that elevations of WSS to levels found in these conditions can cause fragmentation of the internal elastic lamina of blood vessels (Steiger 1990), as well as alterations in endothelial phenotype or endothelial damage (Stehbens 1989). Additionally, increased flow and systemic hypertension are required to create experimental cerebral aneurysms in rats and primates (Hashimoto et al. 1980, Kim et al. 1989, Kondo 1997, Nagata et al. 1980).

2.5. Aneurysm Progression

Despite the agreement on the mechanism of aneurysm initiation, there is significant controversy regarding the mechanisms responsible for the growth and ultimate rupture of a cerebral aneurysm, with two main schools of thought: high-flow effects and low-flow effects. In each theory, the hemodynamic environment within the aneurysm interacts with the cellular elements of the aneurysmal wall to cause a weakening of the wall. From histological observations, investigators concluded that the mechanical properties of the aneurysmal wall are mainly related to collagen. Measurements of the strength of the aneurysm walls from cadaveric and surgical specimens demonstrated that the yield stress of tissue in the fundi of aneurysms was mildly in excess of the calculated systolic stresses in contrast to the normal arterial wall, which were higher by a factor of 10 to 20 (Steiger et al. 1989). Furthermore, this analysis showed that the stress tolerated by aneurysm walls for a prolonged period was in the range of the stress imposed in vivo by the mean blood pressure. Therefore, aneurysm growth could be understood as a passive yield to blood pressure and reactive healing and thickening of the wall with increasing aneurysm diameter. The distinguishing feature between the two schools of thought is in the mechanisms responsible for wall weakening.

The high-flow theory focuses on the effects of WSS elevation. Elevation of maximal WSS can cause endothelial injury and thus initiates wall remodeling and potential degeneration (Nakatani et al. 1991). A vascular endothelium malfunction and/or an abnormal shear stress field can cause an overexpression of endothelium-dependent NO production, which leads to a lower, nonphysiological local arterial tone via processes connected to the scarcity and apoptosis of wall-embedded smooth muscle cells and wall remodeling (Fukuda et al. 2000, Guzman et al. 1997, Hara et al. 1998, Sho et al. 2001). This results in a disturbance of the equilibrium between the blood-pressure forces and the internal wall stress forces, in favor of the former, and subsequently dilates the arterial wall locally. The resulting abnormal blood shear stress

field is the driving factor for further growth of the aneurysmal geometry. This geometrical growth stretches the collagen and elastin fibers of the medial and adventitial layers and gives rise to internal stresses that contribute to the arterial stiffness. Eventually, the biomechanical system equilibrates at a state at which the internal wall stresses and the transmural pressure are equal while the local hemodynamics cannot alter the arterial properties any more. At this point, the elastin and the collagen fibers are constantly under a nonphysiologically large mechanical load and eventually undergo remodeling.

The low-flow theory points to low flows within aneurysms as the cause of localized blood-flow stagnation against the wall in the dome. Blood stagnation causes a dysfunction of flow-induced NO, which is usually released by mechanical stimulation from increased shear stress. This dysfunction results in the aggregation of red blood cells, as well as the accumulation and adhesion of both platelets and leukocytes along the intimal surface (Griffith 1994, Liepsch 1986, Moncada et al. 1991, Moritake et al. 1973). This process may cause intimal damage, leading to the infiltration of white blood cells and fibrin inside the aneurysm wall, all of which have been seen in pathological examinations of aneurysm walls (Crawford 1959, Crompton 1966). The inflammation leads to the localized degeneration of the aneurysm wall, resulting in a lower pressure threshold at which physiological tensile forces could be supported. The aneurysm wall progressively thins and finally may cause the tissue to tear.

2.6. Peri-Aneurysmal Environment Factors

The evolution of an aneurysm (its final shape or rupture) results from the interplay among the intravascular forces, the mechanical properties of the aneurysm wall, and their interaction with the structures around the aneurysm, which is known as the peri-aneurysmal environment (PAE). As an aneurysm grows, it comes in contact with structures in the peri-aneurysmal space such as bone, brain tissue, nerves, and dura. Symptoms related to this interaction are well known clinically, manifesting as bone erosion, obstructive hydrocephalus, and cranial nerve palsy (Hongo et al. 2001, Platania et al. 2002), and indicate the pressure exerted by the aneurysm in contact with the surrounding structures. However, the PAE's effect on aneurysm evolution is poorly understood. Using finite-element analyses of stress fields in a mathematical model, Seshaiyer & Humphrey (2001) have shown that certain distributions of contact constraints in some aneurysm geometries may decrease stresses and provide a protective effect. Using high-resolution computed-tomography imaging, Ruiz et al. (2006) showed that contact constraints from the PAE influence both aneurysm shape and the risk of rupture. They associated balanced contact with unruptured aneurysms and unbalanced or absent contact with ruptured aneurysms. Logically, the expansion of the aneurysm should eventually lead to contact with surrounding structures that locally reinforce the wall and resist further expansion. However, as with hemodynamic factors such as WSS, contact is not uniformly distributed around the aneurysm wall, leading to a potentially complex interaction between wall-damaging mechanisms and peri-aneurysmal support. The result of this could be either protective or detrimental for the evolution of the aneurysm.

3. Cerebral Hemodynamics

3.1. Modeling Hemodynamics

The blood-flow dynamics of cerebral aneurysms have been studied in numerous experimental models and clinical studies to investigate the role of hemodynamics in the initiation, growth, and rupture of aneurysms (Burleson et al. 1995, Gobin et al. 1994, Gonzalez et al. 1992, Liou & Liou 1999, Nakatani et al. 1991, Satoh et al. 2003, Tateshima et al. 2001, Tenjin et al. 1998, Ujiie et al. 1999). Although this work has characterized the complexity of intra-aneurysmal hemodynamics, the studies have largely focused on idealized aneurysm geometries or surgically created aneurysms in animals. Each of these previous approaches has had

significant limitations in connecting the hemodynamic factors studied to clinical events. In vitro studies using idealized geometries have allowed detailed measurement of hemodynamic variables (Liou & Liou 1999) but cannot be used directly to understand the hemodynamic forces in an individual clinical case.

Computationally based models circumvent this problem owing to their ability to study all possible geometries (Cebral et al. 2004, Hassan et al. 2004, Jou et al. 2003, Steinman et al. 2003). Although current imaging modalities are limited for the in vivo quantification of blood-flow patterns, the geometrical shape of aneurysms can be accurately reconstructed from anatomical images. This has allowed the application of computational fluid dynamics (CFD) techniques in subject-specific geometries extracted from medical images (Butty et al. 2002, Cebral et al. 2004, Hassan et al. 2004, Jou et al. 2003, Steinman et al. 2003). A number of experimental studies have also been carried out with realistic anatomical models constructed from images using rapid prototyping techniques (Tateshima et al. 2001, 2003a,b). Using simulated or virtual angiograms, researchers recently showed that image-based patient-specific computational models are capable of reproducing the flow structures in cerebral aneurysms observed in vivo during angiographic examinations (Cebral et al. 2007, Ford et al. 2005b).

Most CFD modeling approaches approximate blood flow as a continuous incompressible fluid. The corresponding mathematical model is described by the three-dimensional unsteady incompressible Navier-Stokes equations (Mazumdar 1992) (see Figure 1). Newtonian models may provide a reasonable approximation for blood flow in large arteries (Perktold et al. 1991, Perktold & Rappitsch 1995, Steinman 2004, Stuhne & Steinman 2004, Taylor & Draney 2004, Zhao et al. 2000). However, for aneurysmal flows, this approximation may be not entirely justified because of the presence of slow-flow regions in which non-Newtonian properties become important (Basombrio et al. 2000). A number of non-Newtonian models have been developed to approximate the observed rheological behavior of blood (Mazumdar 1992) and have been incorporated into patient-based models (Cebral et al. 2005a). Although many hemodynamic studies consider vessel compliance to be a second-order effect and neglect it (Perktold & Rappitsch 1994, 1995; Steinman 2004; Taylor & Draney 2004), its influence on in vivo intra-aneurysmal flow patterns has not been characterized (Shojima et al. 2004). Fluid-structure interaction algorithms have been developed to incorporate wall compliance into the vascular CFD models (Cebral et al. 2002, Taylor & Draney 2004, Zeng & Ethier 2003, Zeng et al. 2003, Zhao et al. 2000). However, this is a challenging problem because it requires knowledge about the distribution of wall thickness, wall elasticity, and intra-arterial pressure waveform (Cebral 2002, Cebral et al. 2002). In a recent study, the pulsation of the wall was measured using dynamic angiography images and nonrigid registration algorithms and was imposed as a boundary condition in CFD models (Dempere-Marco et al. 2006, Oubel et al. 2007). Although the WSS and velocity magnitudes were affected by the wall motion, the main characteristics of the flow patterns (such as location and size of the inflow jet and the complexity and stability of the intra-aneurysmal flow pattern) were not significantly altered.

3.2. Hemodynamics in the Circle of Willis

The study of blood flows in normal cerebral arteries and the circle of Willis is essential for a better understanding of the local hemodynamics environment in which aneurysms form and develop. Several studies of the hemodynamics in the circle of Willis have been carried out using computational models (Alastruey et al. 2007, Alnaes et al. 2007, Cassot et al. 2000, Cebral et al. 2003, Ferrandez et al. 2000). A recent study used CFD to investigate the impact of variations in vessel radii and bifurcation angles on pressure and WSS in the complete circle of Willis (Alnaes et al. 2007). The authors found that deviations from normal anatomy result in a redistribution of wall pressures and increased WSS at branch points. One weakness in this interesting study is the use of idealized geometries, which could be overcome by using patient-

based models of the complete circle of Willis (Cebral et al. 2003). Recently, four-dimensional phase-contrast magnetic resonance techniques have been used to image in vivo blood-flow patterns in cerebral arteries of normal subjects (Bammer et al. 2007, Wetzel et al. 2007). Both the in vivo imaging and computational modeling studies have characterized the complexities of the blood-flow patterns and WSS distributions in the major cerebral arteries. In particular, they have demonstrated the nonuniform distribution of WSS along the vessels, with increased and decreased zones at arterial bifurcations and regions of high vessel curvature, which coincide with the most common locations for aneurysm development (Brisman et al. 2006). Helical or swirling flows (also called secondary flows) induced by the curving geometry of the cerebral arteries are fundamentally important because they govern the local distribution of WSS forces acting on the vessel walls. Figure 2 illustrates the hemodynamic characteristics of the major cerebral vessels, showing CFD models constructed from phase-contrast magnetic resonance images of a normal subject and the corresponding blood-flow pattern and WSS distribution at peak systole.

3.3. Hemodynamics in Cerebral Aneurysms

Numerous computational and experimental studies of cerebral aneurysms have been carried out using realistic geometries obtained from medical images (Cebral et al. 2005b, Hassan et al. 2004, Jou et al. 2003, Kerber et al. 1999, Shojima et al. 2004, Steinman et al. 2003, Tateshima et al. 2003a, Valencia & Solis 2006). These investigations reveal a wide variety of complex intra-aneurysmal flow patterns that are strongly dependent on the patient-specific vascular geometry and thus are not easily predictable by a simple inspection or by extrapolation from idealized models.

The intra-aneurysmal flow patterns range from those that are simple and stable to those that are complex and unstable (or turbulent). Simple flow patterns consist of a single recirculation region or a vortical structure within the aneurysm. This main vortex can remain stable or move during the cardiac cycle. More complex flow patterns contain more than one recirculation region that can remain stable, move, or become intermittent during the cardiac cycle. Figure 3 presents examples of intra-aneurysmal flow patterns with different degrees of complexity.

The intra-aneurysmal flow structures depend not only on the size and shape of the aneurysm but also on the way the blood flows from the parent vessel into the aneurysm, which in turn is influenced by the geometry of the parent artery. In some aneurysms, the blood flows from the parent vessel directly into the aneurysm, resulting in a concentrated inflow jet that impacts the aneurysm wall, producing a region of locally elevated WSS. Other aneurysms have a more diffuse inflow jet that produces a slower intra-aneurysmal flow pattern and a more uniform WSS distribution, with magnitudes typically lower than those of the parent vessels. Examples of aneurysms with concentrated and diffuse inflow jets and the corresponding WSS distributions are shown in Figure 4. The regions of elevated WSS can be small or large relative to the aneurysm size, depending on whether the inflow jet is concentrated or diffuse.

The blood flow in the curved arteries of the brain is characterized by strong secondary flows that create swirling helical patterns. These patterns determine the location of the inflow portion of the aneurysm neck, as well as the location and size of the impact zone on the aneurysm wall. In contrast with idealized models that place the inflow at the distal part of the aneurysm neck, patient-specific models show that the inflow can also be located on the sides or at the proximal part of the neck. Examples of aneurysms with different inflow locations are shown in Figure 5.

The impingement of the inflow jet against the aneurysm wall produces a local elevation of the WSS. Depending on the geometric configuration of the aneurysm with respect to the parent

artery, the zone of flow impingement can be located at the neck, the body, or the dome of the aneurysm (Figure 6).

3.4. Hemodynamics and Cerebral Aneurysm Evolution

Computational models have provided some insight into mechanisms for aneurysm rupture, although explanations for these mechanisms differ. Proponents of the low–shear stress theories rely on several clinical observations and CFD data they consider to be incompatible with the high–shear stress mechanisms. First, prior CFD modeling has shown that focal elevations in WSS are largely confined to the downstream lip of an aneurysm, yet the dome is clinically the most common site of rupture (Suzuki & Ohara 1978), and WSS in the dome is low. Thus, they reason, shear stress can be related to aneurysm growth only if one assumes that the active matrix of aneurysm growth is located at the orifice. However, angiographically documented cases of aneurysm growth generally show progression of the dome but only rarely changes in the neck region (Ono et al. 1985). Second, the strongest known predictor of an aneurysm's rate of rupture is size, with larger sizes corresponding to elevated rates of rupture. Flow velocities in aneurysms depend on the volume, with velocity being inversely proportional to the square of the maximum diameter of the fundus (Liepsch et al. 1987; Perktold et al. 1989; Steiger & Reulen 1986; Steiger et al. 1987, 1988). Moreover, a direct relationship exists between the area of the orifice and the intra-aneurysmal flow velocities (Black & German 1960). These observations have led to a clinical measure called the aspect ratio (which is the depth of aneurysm divided by the neck width). Some studies have found an aspect ratio greater than 1.6 to be correlated with a risk of rupture (Ujiie et al. 2001). Finally, CFD analysis and experimental in vitro measurements of WSS have shown that the WSS magnitude of the aneurysm region is significantly lower than that of the vessel region, and WSS inversely correlates with the aspect ratio (Shojima et al. 2004). Naturally, these authors' conclusion is that high shear stress cannot be the cause of aneurysm rupture.

Despite these admittedly compelling arguments, the low–shear stress theory may not be the best explanation for aneurysm rupture. First, low WSS at the bifurcations of carotid arteries is causally connected with proliferative degenerative alterations (i.e., atheromas). Although atheromas are found in a minority of cerebral aneurysms, their presence is not a common finding in histological examinations of ruptured aneurysms. Why would we anticipate the biological response to be different intra-aneurysmally? Second, much of the previous CFD work was performed using idealized lateral wall aneurysm models that are not representative of the wide range of geometries found in patients. More recent patient-specific CFD modeling (Cebral et al. 2005b,c; Shojima et al. 2004) has shown that the point of flow impingement by the inflow jet is located in the neck region in only a minority of cases. Areas of elevated shear stress are commonly found in the body or dome of an aneurysm (Tateshima et al. 2003a), although the spatial average WSS is lower than the parent artery for most aneurysms. Finally, the size of the wall impingement zone is statistically associated with a prior clinical event of rupture (Cebral et al. 2005b,c). This may imply that the aspect ratio may predict aneurysmal rupture, not as a predictor of low-flow recirculation (i.e., low WSS) but because narrow necks in large aneurysms geometrically induce concentrated inflow jets and small concentrated impaction zones.

4. Concluding Remarks

The role of blood-flow physiological parameters regulating aneurysm morphology and natural history is poorly understood. It is necessary to model intra-aneurysmal hemodynamics using realistic aneurysm geometries because aneurysm geometry is one of the most important factors determining aneurysm flow patterns and WSS distributions that influence aneurysm progression. Most models tend to oversimplify the complex flow patterns observed in aneurysms in vivo. The difficulty of developing reliable in vitro and animal models has

hampered an accurate evaluation of those physiologic parameters. Furthermore, better understanding of the mechanisms of aneurysmal growth requires the study of the interaction among hemodynamics, wall mechanobiology, wall biomechanics, and contacts with the PAE structures. This will help improve patient evaluation and treatment.

Summary Points

1. The rupture of intracranial aneurysms cannot be explained on a purely mechanical basis.
2. The weakening of aneurysmal walls has been demonstrated in histological studies that found degeneration of endothelial cells, degeneration of the internal elastic lamina, and thinning of the medial layer.
3. Aneurysm formation is believed to be caused by the interaction of abnormally high-flow hemodynamic forces (caused by anatomical variations and pathological conditions) and the arterial wall mechanobiology.
4. High-flow theories claim that abnormally high WSS causes an excessive production of NO, which results in lower local arterial tone owing to the scarcity and apoptosis of smooth muscle cells and wall remodeling.
5. Low-flow theories claim that low WSS causes a dysfunction of flow-induced NO, which results in the aggregation of red blood cells and the accumulation and adhesion of platelets and leukocytes, which in turn cause intimal damage and inflammation, leading to localized degeneration of the aneurysm wall.
6. Contacts with extravascular structures play an important role in the evolution of aneurysms and can have a protective or damaging effect on the aneurysm wall.
7. Investigators can make patient-specific image-based hemodynamics models to accurately represent in vivo conditions. These models reveal a wide variety of complex intra-aneurysmal flow patterns that are strongly dependent on the patient-specific vascular geometry and thus are not easily predictable by simple inspection or by extrapolation from idealized models.

Future Directions

1. Researchers need to develop realistic models of aneurysm growth that combine hemodynamics, biomechanics, mechanobiology, and the PAE.
2. Researchers also need to correlate model-predicted variables with clinical observations to further understand the mechanisms responsible for aneurysm evolution and rupture.

Acknowledgments

We thank the National Institutes of Health, the American Heart Association, Philips Medical Systems, and Boston Scientific for financial support.

Disclosure Statement: J.R.C. is partially supported from research grants from Philips Medical Systems and Boston Scientific, and C.M.P. has received funding from Philips Medical Systems.

Literature Cited

Alastruey J, Parker KH, Peiro J, Byrd SM, Sherwin SJ. Modelling the circle of Willis to assess the effects of anatomical variations and occlusions on cerebral flows. J Biomech 2007;40:1794–805. [PubMed: 17045276]

Alnaes MS, Isaksen J, Mardal KE, Rommer B, Morgan MK, Ingebritsen T. Computation of hemodynamics in the circle of Willis. Stroke 2007;38:2500–5. [PubMed: 17673714]

Bammer R, Hope TA, Aksoy M, Alley MT. Time-resolved 3D quantitative flow MRI of the major intracranial vessels: initial experience and comparative evaluation at 1.5T and 3.0T in combination with parallel imaging. Magn Reson Med 2007;57:127–40. [PubMed: 17195166]

Basombrio, F.; Dari, E.; Buscaglia, GC.; Feijoo, RA. Numerical experiments in complex haemodynamics flows: non-Newtonian effects. Presented at XI ENIEF; Bariloche, Argentina. 2000.

Black SPW, German WL. Observation on the relationship between the volume and the size of the orifice of experimental aneurysms. J Neurosurg 1960;17:984–90.

Boecher-Schwarz HG, Ringel K, Kopacz L, Heimann A, Kempski O. Ex vivo study of the physical effect of coils on pressure and flow dynamics in experimental aneurysms. Am J Neuroradiol 2000;21:1532–36. [PubMed: 11003291]

Brisman JL, Song JK, Newell DW. Cerebral aneurysms. N Engl J Med 2006;355:928–39. [PubMed: 16943405]

Bruno G, Todor DR, Lewis I, Chyatte D. Vascular extracellular matrix remodeling in cerebral aneurysms. J Neurosurg 1998;89:431–40. [PubMed: 9724118]

Buonocore MH. Visualizing blood flow patterns using streamlines, arrows, and particle paths. Magn Reson Med 1998;40:210–26. [PubMed: 9702703]

Burleson AC, Strother CM, Turitto VT. Computer modeling of intracranial saccular and lateral aneurysms for the study of their hemodynamics. Neurosurgery 1995;37:774–84. [PubMed: 8559308]

Butty VD, Gudjonsson K, Buchel P, Makhijani VB, Ventikos Y, Poulikakos D. Residence times and basins of attraction for a realistic right internal carotid artery with two aneurysms. Biorheology 2002;39:387–93. [PubMed: 12122257]

Cassot F, Zagzoule M, Marc-Vergnes JP. Hemodynamic role of the circle of Willis in stenosis of internal carotid arteries: an analytical solution to a linear model. J Biomech 2000;33:395–405. [PubMed: 10768388]

Cebral, JR. Realistic modeling of arterial hemodynamics from anatomic and physiologic image data. In: Batra, RC.; Henneke, EG., editors. Proc 14th U S Natl Congr Theor Appl Mech. Blacksburg: Va. Polytech. Inst.; 2002. p. 79

Cebral JR, Castro MA, Appanaboyina S, Putman CM, Millan D, Frangi AF. Efficient pipeline for image-based patient-specific analysis of cerebral aneurysm hemodynamics: technique and sensitivity. IEEE Trans Med Imaging 2005a;24:457–67. [PubMed: 15822804]

Cebral JR, Castro MA, Burgess JE, Pergolizzi R, Sheridan MJ, Putman CM. Characterization of cerebral aneurysm for assessing risk of rupture using patient-specific computational hemodynamics models. Am J Neuroradiol 2005b;26:2550–59. [PubMed: 16286400]

Cebral JR, Castro MA, Millan D, Frangi AF, Putman CM. Pilot clinical investigation of aneurysm rupture using image-based computational fluid dynamics models. Proc SPIE Med Imaging 2005c;5746:245–56.

Cebral JR, Castro MA, Soto O, Löhner R, Alperin N. Blood flow models of the circle of Willis from magnetic resonance data. J Eng Math 2003;47:369–86.

Cebral JR, Hernandez M, Frangi AF, Putman CM, Pergolizzi R, Burgess JE. Subject-specific modeling of intracranial aneurysms. Proc SPIE Med Imaging 2004;5369:319–27.

Cebral JR, Pergolizzi R, Putman CM. Computational fluid dynamcis modeling of intracranial aneurysms: qualitatively comparison with cerebral angiography. Acad Radiol 2007;14:804–13. [PubMed: 17574131]

Cebral JR, Yim PJ, Löhner R, Soto O, Choyke PL. Blood flow modeling in carotid arteries using computational fluid dynamics and magnetic resonance imaging. Acad Radiol 2002;9:1286–99. [PubMed: 12449361]

Chyatte D, Lewis I. Gelatinase activity and the occurrence of cerebral aneurysms. Stroke 1997;28:799–804. [PubMed: 9099199]

Crawford T. Some observations of the pathogenesis and natural history of intracranial aneurysms. J Neurol Neurosurg Psychiatry 1959;22:259–66. [PubMed: 13812726]

Crompton M. Mechanism of growth and rupture in cerebral berry aneurysms. Br Med J 1966;1:1138–42. [PubMed: 5932074]

Dardik A, Chen L, Frattini J, Asada H, Aziz F, et al. Differential effects of orbital and laminar shear stress on endothelial cells. J Vasc Surg 2005;41:869–80. [PubMed: 15886673]

Dempere-Marco L, Oubel E, Castro MA, Putman CM, Frangi AF, Cebral JR. Estimation of wall motion in intracranial aneurysms and its effects on hemodynamic patterns. Lect Notes Comp Sci 2006;4191:438–45.

Drexler H, Hornig B. Endothelial dysfunction in human disease. J Mol Cell Cardiol 1999;31:51–60. [PubMed: 10072715]

Ferrandez A, David T, Bamford J, Scott J, Guthrie A. Computational models of blood flow in the circle of Willis. Comp Methods Biomech Biomed Eng 2000;4:1–26.

Ford MD, Alperin N, Lee SH, Holdsworth DW, Steinman DA. Characterization of volumetric flow rate waveforms in the normal internal carotid and vertebral arteries. Physiol Meas 2005a;26:477–88. [PubMed: 15886442]

Ford MD, Stuhne GR, Nikolov HN, Habets DF, Lownie SP, et al. Virtual angiography for visualization and validation of computational models of aneurysm hemodynamics. IEEE Trans Med Imaging 2005b;24:1586–92. [PubMed: 16350918]

Friedman M, Hutchins G, Bargeron C, Deters O, Mark F. Correlation between intimal thickness and fluid shear in human arteries. Atherosclerosis 1981;39:425–36. [PubMed: 7259822]

Fukuda S, Hashimoto N, Naritomi H, Nagata I, Nozaki K, et al. Prevention of rat cerebral aneurysm formation by inhibition of nitric oxide synthase. Circulation 2000;101:2532–38. [PubMed: 10831529]

Gobin YP, Counard JL, Flaud P. In vitro study of haemodynamics in a giant saccular aneurysm model: influence of flow dynamics in the parent vessel and effects of coil embolization. Neuroradiology 1994;36:530–36. [PubMed: 7845578]

Gonzalez CF, Choi YI, Ortega V. Intracranial aneurysms: flow analysis of their origin and progression. Am J Neuroradiol 1992;13:181–88. [PubMed: 1595440]

Griffith TM. Modulation of blood flow and tissue perfusion by endothelium-derived relaxing factor. Exp Physiol 1994;779:873–913. [PubMed: 7873159]

Groden C, Laudan J, Gatchell S, Zeumer H. Three-dimensional pulsatile flow simulation before and after endovascular coil embolization of a terminal cerebral aneurysm. J Cereb Blood Flow Metab 2001;21:1464–71. [PubMed: 11740208]

Guzman RJ, Abe K, Zarins C. Flow-induced arterial enlargement is inhibited by suppresion of nitric oxide synthase activity in vivo. Surgery 1997;122:273–79. [PubMed: 9288132]

Hara A, Yoshimi N, Mori H. Evidence for apoptosis in human intracranial aneurysms. Neurol Res 1998;20:127–30. [PubMed: 9522347]

Hashimoto N, Handa H, Nagata I, Hazama F. Experimentally induced cerebral aneurysms in rats: Part V. Relation of hemodynamics in the circle of Willis to formation of aneurysms. Surg Neurol 1980;13:41–45. [PubMed: 7361257]

Hassan T, Ezura M, Timofeev EV, Tominaga T, Saito T, et al. Computational simulation of therapeutic parent artery occlusion to treat giant vertebrobasilar aneurysm. Am J Neuroradiol 2004;25:63–68. [PubMed: 14729530]

Hongo K, Morota N, Watabe T. Giant basilar bifurcation aneurysm presenting as a third ventricular mass with unilateral obstructive hydrocephalus: case report. J Clin Neurosci 2001;8:51–54. [PubMed: 11148080]

Jou LD, Quick CM, Young WL, Lawton MT, Higashida R, et al. Computational approach to quantifying hemodynamic forces in giant cerebral aneurysms. Am J Neuroradiol 2003;24:1804–10. [PubMed: 14561606]

Kaminogo M, Yonekura M, Shibata S. Incidence and outcome of multiple intracranial aneurysms in a defined population. Stroke 2003;34:16–21. [PubMed: 12511744]

Kamiya A, Ando J, Shibata S, Matsuda H. Roles of fluid shear stress in physiological regulation of vascular structure and function. Biorheology 1988;25:271–78. [PubMed: 3196824]

Kassell NF, Torner JC, Haley ECJ, Jane JA, Adams HP, Kongable GL. The international cooperative study on the timing of aneurysm surgery. Part 1: overall management results. J Neurosurg 1990;73:18–36. [PubMed: 2191090]

Kayembe KNT, Sasahara M, Hazama F. Cerebral aneurysms and variations of the circle of Willis. Stroke 1984;15:846–50. [PubMed: 6474536]

Kerber CW, Heilman CB. Flow in experimental berry aneurysms: method and model. Am J Neuroradiol 1983;4:374–77. [PubMed: 6410748]

Kerber CW, Imbesi SG, Knox K. Flow dynamics in a lethal anterior communicating artery aneurysm. Am J Neuroradiol 1999;20:2000–3. [PubMed: 10588134]

Kim C, Kikuchi H, Hashimoto N, Hazama F, Kataoka H. Establishment of experimental conditions for inducing saccular cerebral aneurysms in primates with special reference to hypertension. Acta Neurchir (Wein) 1989;96:132–36.

Kojima M, Handa N, Hashimoto N. Early changes of experimentally induced cerebral aneurysms in rat: scanning electron microscopic study. Stroke 1986;17:835–41. [PubMed: 3764951]

Kondo S. Cerebral aneurysms arising at nonbranching sites: an experimental study. Stroke 1997;28:398–403. [PubMed: 9040697]

Kondo S, Hashimoto N, Kikuchi H. Apoptosis of medial smooth muscle cells in the development of saccular cerebral aneurysms in rats. Stroke 1998;29:181–89. [PubMed: 9445349]

Ku DN, Giddens DP, Zarins C, Glagov S. Puslatile flow and atherosclerosis in the human carotid bifurcation: positive correlation between plaque location and low oscillating shear stress. Atherosclerosis 1985;5:293–302.

Kyriacou SK, Humphrey JD. Influence of size, shape and properties on the mechanics of axisymmetric saccular aneurysms. J Biomech 1996;29:1015–22. [PubMed: 8817368]

Liepsch DW. Flow in tubes and arteries: a comparison. Biorheology 1986;23:395–433. [PubMed: 3779064]

Liepsch DW, Steiger HJ, Poll A, Reulen HJ. Hemodynamic stress in lateral saccular aneurysms. Biorheology 1987;24:689–710. [PubMed: 2971404]

Linn FH, Rinkel GJ, Algra A, van Gijn J. Incidence of subarachnoid hemorrhage: role of region, year, and rate of computed tomography. A meta-analysis. Stroke 1996;27:625–29. [PubMed: 8614919]

Liou TM, Liou SN. A review of in vitro studies of hemodynamic characteristics in terminal and lateral aneurysm models. Proc Natl Sci Counc Repub China B 1999;23:133–48. [PubMed: 10518314]

Luscher TF, Tanner FC. Endothelial regulation of vascular tone and growth. Am J Hypertens 1993;6:S283–93.

Matsuda M, Handa J, Saito A, Matsuda I, Kamijyo Y. Ruptured cerebral aneurysms associated with arterial occlusion. Surg Neurol 1983;20:4–12. [PubMed: 6867926]

Mazumdar, J. Biofluid Mechanics. Singapore: World Sci.; 1992.

Metcalfe RW. The promise of computational fluid dynamics as a tool for delineating therapeutic options in the treatment of aneurysms. Am J Neuroradiol 2003;24:553–54. [PubMed: 12695178]

Moncada S, Plamer RMJ, Higgs EA. Nitric oxide: physiology, pathology and pharmacology. Pharmacol Rev 1991;43:109–42. [PubMed: 1852778]

Moritake K, Handa H, Hayashi K, Sato M. Experimental studies on intracranial aneurysms (a preliminary report): some biomechanical considerations on the wall structures of intracranial aneurysms and experimentally produced aneurysms. No Shinkei Sheka 1973;1:115–23.

Nagata I, Handa H, Hashimoto N, Hazama F. Experimentally induced cerebral aneruysms in rats: VI, hypertension. Surg Neurol 1980;14:477–79. [PubMed: 6111849]

Nakatani H, Hashimoto N, Kang Y, Yamazoe N, Kikuchi H, et al. Cerebral blood flow patterns at major vessel bifurcations and aneurysms in rats. J Neurosurg 1991;74:258–62. [PubMed: 1988596]

Onda H, Kasuya H, Yoneyama T. Genomewide-linkage and haplotype-association studies map intracranial aneurysm to chromosome 7q11. Am J Hum Genet 2001;69:804–19. [PubMed: 11536080]

Ono N, Imai S, Zama A, Hoska T, Onoda K, Wakao T. Clinical significance of short-term cerebral aneurysm enlargement. Neurol Med Chir (Tokyo) 1985;25:534–40. [PubMed: 2415846]

Ortega HV. Computer simulation helps predict cerebral aneurysms. J Med Eng Technol 1998;22:179–81. [PubMed: 9680602]

Oubel E, DeCraene M, Putman CM, Cebral JR, Frangi AF. Analysis of intracranial aneurysm wall motion and its effects on hemodynamic patterns. Proc SPIE Med Imaging 2007;6511:65112A.

Peerless, SJ.; Drake, CG. Management of aneurysms of the posterior circulation. In: Youmans, JR., editor. Neurological Surgery. Vol. 3. New York: Saunders; 1982. p. 1715-63.

Perktold K, Peter R, Resch M. Pulsatile non-Newtonian blood flow simulation through a bifurcation with an aneurysm. Biorheology 1989;26:1011–30. [PubMed: 2624892]

Perktold K, Peter RO, Resch M, Langs G. Pulsatile non-Newtonian blood flow in three-dimensional carotid bifurcation models: a numerical study of flow phenomena under different bifurcation angles. J Biomed Eng 1991;13:507–15. [PubMed: 1770813]

Perktold, K.; Rappitsch, G. Mathematical modeling of local arterial flow and vessel mechanics. In: Crolet, J.; Ohayon, R., editors. Computational Methods for Fluid-Structure Interaction. Harlow, UK: Longman Sci. Tech.; 1994. p. 230-45.

Perktold, K.; Rappitsch, G. Computer simulation of arterial blood flow: vessel diseases under the aspect of local hemodynamics. In: Jaffrin, MY.; Caro, CG., editors. Biological Flows. New York: Plenum; 1995. p. 83-114.

Platania N, Cutuli V, Nicoletti G. Oculomotor palsy and supraclinoid internal carotid artery aneurysms: personal experience and review of the literature. J Neurosurg Sci 2002;46:107–10. [PubMed: 12690332]

Ruiz D, Yilmaz H, Dehashti AR, Alimenti A, de Tribolet N, Rufenacht DA. The perianeurysmal environment: influence on saccular aneurysm shape and rupture. Am J Neuroradiol 2006;27:504–12. [PubMed: 16551985]

Salar G, Mingrino S. Ligature of the cervical carotid artery for the treatment of intracranial carotid aneurysms: complications and late results. Acta Neurochir (Wein) 1977;36:152.

Salar G, Mingrino S. Development of intracranial saccular aneurysms: report of two cases. Neurosurgery 1981;8:462–65. [PubMed: 7242899]

Satoh T, Onoda K, Tsuchimoto S. Visualization of intraaneurysmal flow patterns with transluminal flow images of 3D MR angiograms in conjunction with aneurysmal configurations. Am J Neuroradiol 2003;24:1436–45. [PubMed: 12917142]

Seshaiyer P, Humphrey JD. On the potentially protective role of contact constraints on saccular aneurysms. J Biomech 2001;34:607–12. [PubMed: 11311701]

Sho E, Sho M, Singh TM, Xu C, Zarins C, Masuda H. Blood flow decrease induces apoptosis of endothelial cells in previously dilated arteries resulting from chromic high blood flow. Arterioscler Thromb Vasc Biol 2001;21:1139–45. [PubMed: 11451742]

Shojima M, Oshima M, Takagi K, Torii R, Hayakawa M, et al. Magnitude and role of wall shear stress on cerebral aneurysm: computational fluid dynamic study of 20 middle cerebral artery aneurysms. Stroke 2004;35:2500–5. [PubMed: 15514200]

Stehbens WE. Histopathology of cerebral aneurysms. Arch Neurol 1963;8:272–85. [PubMed: 13983641]

Stehbens, WE. Intracranial aneurysms. In: Stehbens, WE., editor. Pathology of the Cerebral Blood Vessels. St. Louis: Mosby; 1972. p. 351-470.

Stehbens WE. Etiology of intracranial berry aneurysms. J Neurosurg 1989;70:823–31. [PubMed: 2654334]

Steiger HJ. Pathophysiology of development and rupture of cerebral aneurysms. Acta Neurochir (Wein) 1990;48(Suppl):1–57.

Steiger HJ, Auslid R, Keller S, Reulen HJ. Strength, elasticity and viscoelastic properties of cerebral aneurysms. Heart Vessels 1989;5:41–46. [PubMed: 2584177]

Steiger HJ, Poll A, Liepsch D, Reulen HJ. Basic flow structure in saccular aneurysms: a flow visualization study. Heart Vessels 1987;3:55–65. [PubMed: 3500943]

Steiger HJ, Poll A, Liepsch D, Reulen HJ. Haemodynamic stress in terminal aneurysms. Acta Neurochir (Wein) 1988;93:12–23.

Steiger HJ, Reulen HJ. Low frequency flow fluctuations in human saccular aneurysms. Acta Neurochir (Wein) 1986;83:131–37. [PubMed: 2949490]

Steinman DA. Image-based CFD modeling in realistic arterial geometries. Ann Biomed Eng 2004;30:483–97. [PubMed: 12086000]

Steinman DA, Milner JS, Norley CJ, Lownie SP, Holdworth DW. Image-based computational simulation of flow dynamics in a giant intracranial aneurysm. Am J Neuroradiol 2003;24:559–66. [PubMed: 12695182]

Stuhne GR, Steinman DA. Finite element modeling of the hemodynamics of stented aneurysms. J Biomech Eng 2004;126:382–87. [PubMed: 15341176]

Suzuki J, Ohara H. Clinicopathological study of cerebral aneurysms. J Neurosurg 1978;48:505–14. [PubMed: 632875]

Tateshima S, Murayama Y, Villablanca JP. Intraaneurysmal flow dynamics study featuring an acrylic aneurysm model manufactured using computerized tomography angiogram as a mold. J Neurosurg 2001;95:1020–27. [PubMed: 11765817]

Tateshima S, Murayama Y, Villablanca JP, Morino T, Nomura K, et al. In vitro measurement of fluid-induced wall shear stress in unruptured cerebral aneurysms harboring blebs. Stroke 2003a;34:187–92. [PubMed: 12511772]

Tateshima S, Vinuela F, Villablanca JP, Murayama Y, Morino T, et al. Three-dimensional blood flow analysis in a wide-necked internal carotid artery–ophthalmic artery aneurysm. J Neurosurg 2003b; 99:526–33. [PubMed: 12959441]

Taylor CA, Draney MT. Experimental and computational methods in cardiovascular fluid mechanics. Annu Rev Fluid Mech 2004;36:197–231.

Tenjin H, Asakura F, Nakahara Y. Evaluation of intraaneurysmal blood velocity by time-density curve analysis and digital subtraction angiography. Am J Neuroradiol 1998;19:1303–7. [PubMed: 9726473]

Ujiie H, Tachibana H, Hiramtsu O. Effects of size and shape (aspect ratio) on the hemodynamics of saccular aneurysms: a possible index for the surgical treatment of intracranial aneurysms. Neurosurgery 1999;45:119–30. [PubMed: 10414574]

Ujiie H, Tamano Y, Sasaki K, Hori T. Is the aspect ratio a reliable index for predicting the rupture of a saccular aneurysm? Neurosurgery 2001;48:495–503. [PubMed: 11270538]

Valencia A, Solis F. Blood flow dynamics and arterial wall interaction in a saccular aneurysm model of the basilar artery. Comput Struct 2006;84:1326–37.

Wasserman SM. Adaptation of the endothelium to fluid flow: in vitro analyses of gene expression and in vivo implications. Vasc Med 2004;9:34–45.

Weir B. Unruptured intracranial aneurysms: a review. J Neurosurg 2002;96:3–42. [PubMed: 11794601]

Wetzel S, Meckel S, Frydrychowicz A, Bonati L, Radue EW, et al. In vivo assessment and visualization of intracranial arterial hemodynamics with flow-sensitized 4D MR imaging at 3T. Am J Neuroradiol 2007;28:433–38. [PubMed: 17353308]

Wiebers DO, Piepgras DG, Meyer FB, Kallmes DF, Meissner IF, et al. Pathogenesis, natural history, and treatment of unruptured intracranial aneurysms. Mayo Clin Proc 2004;79:1572–83. [PubMed: 15595346]

Winn HR, Jane JA, Taylor J, Kaiser D, Britz GW. Prevalence of asymptomatic incidental aneurysms: review of 4568 arteriograms. J Neurosurg 2002;96:43–49. [PubMed: 11794602]

Yasargil, MG. Microneurosurgery. Vol. 2. New York: Georg Thieme Verlag; 1984.

Zeng D, Ding Z, Friedman MH, Ethier CR. Effects of cardiac motion on right coronary artery hemodynamics. Ann Biomed Eng 2003;31:420–29. [PubMed: 12723683]

Zeng D, Ethier CR. A mesh updating scheme for hemodynamic simulations in vessels undergoing large deformations. J Eng Math 2003;47:405–18.

Zhao SZ, Xu XY, Hughes AD, Thom SA, Stanton AV, et al. Blood flow and vessel mechanics in a physiologically realistic model of a human carotid arterial bifurcation. J Biomech 2000;33:975–84. [PubMed: 10828328]

Glossary

WSS
wall shear stress

NO
nitric oxide

PAE
peri-aneurysmal environment

CFD
computational fluid dynamics

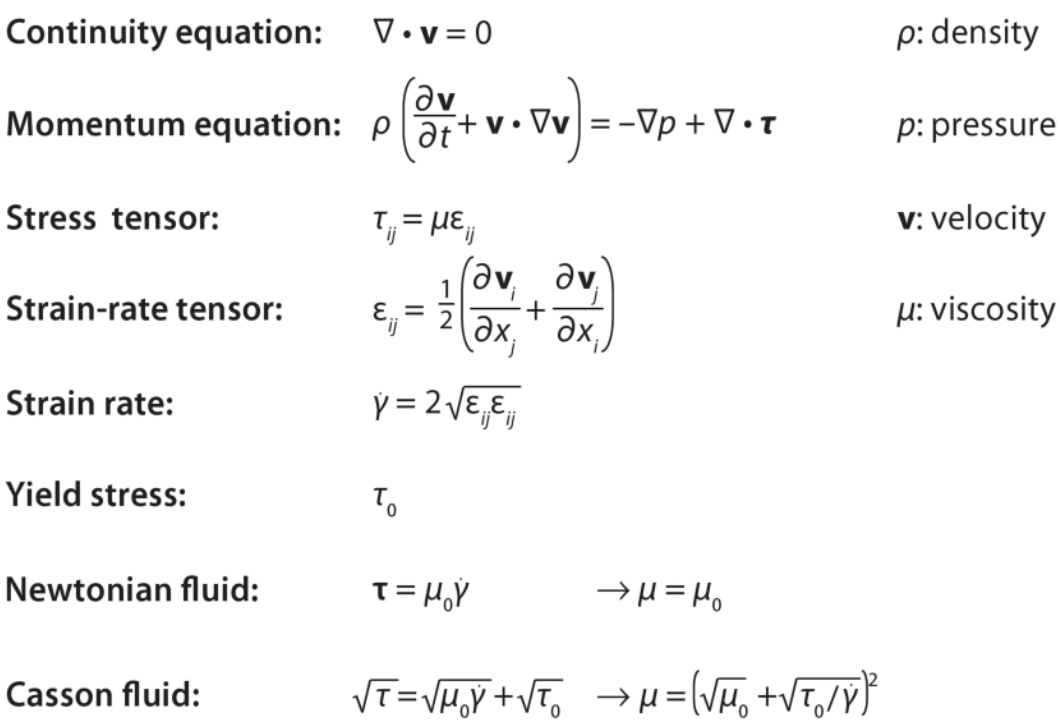

Figure 1.
Mathematical model of blood flows.

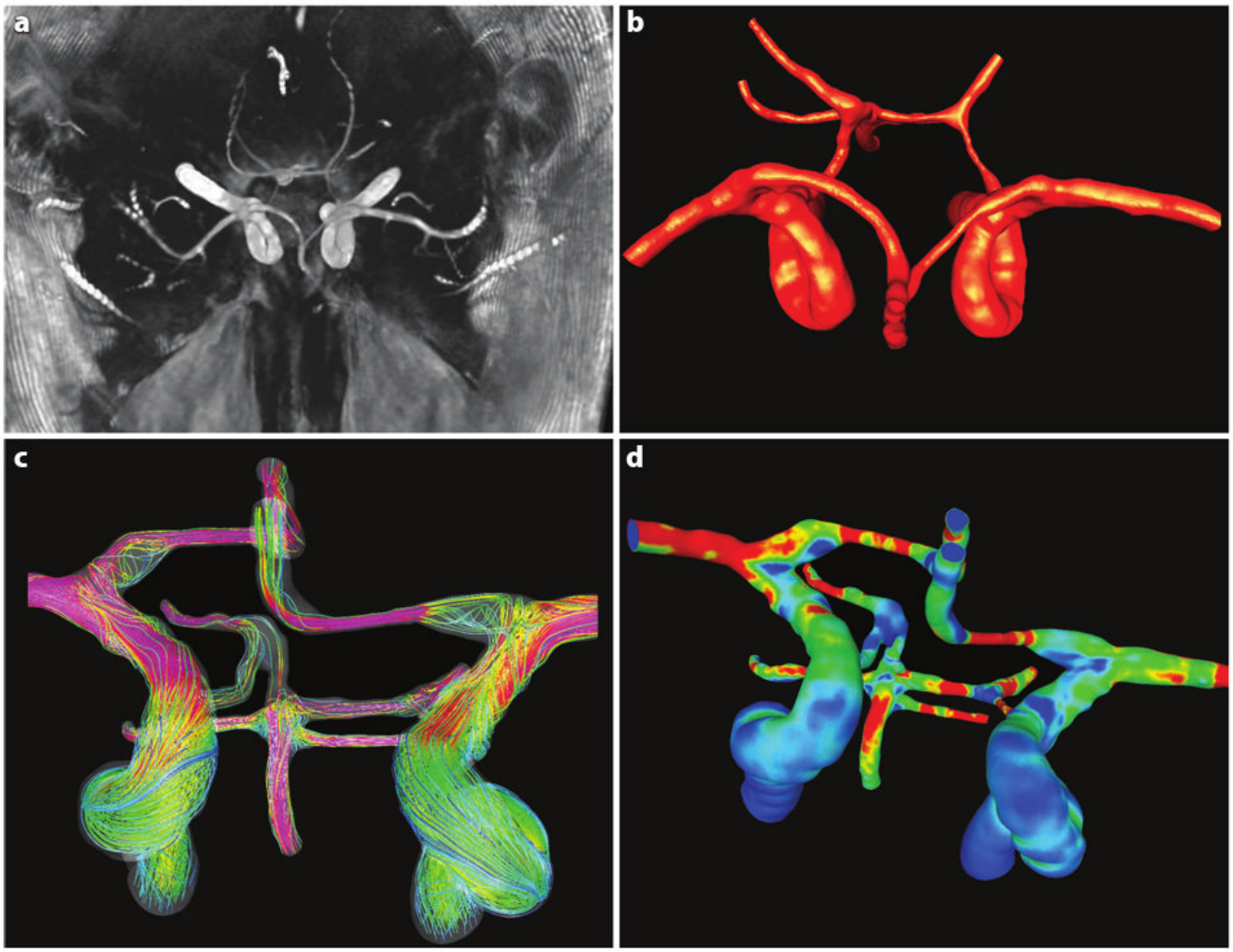

Figure 2.
Computational model of the hemodynamics in the circle of Willis of a normal subject. (*a*) Original medical image and (*b*) corresponding vascular model. (*c*) The complex swirling flows and (*d*) nonuniform wall shear stress (WSS) distribution (with *red* representing the highest WSS) along the major cerebral vessels.

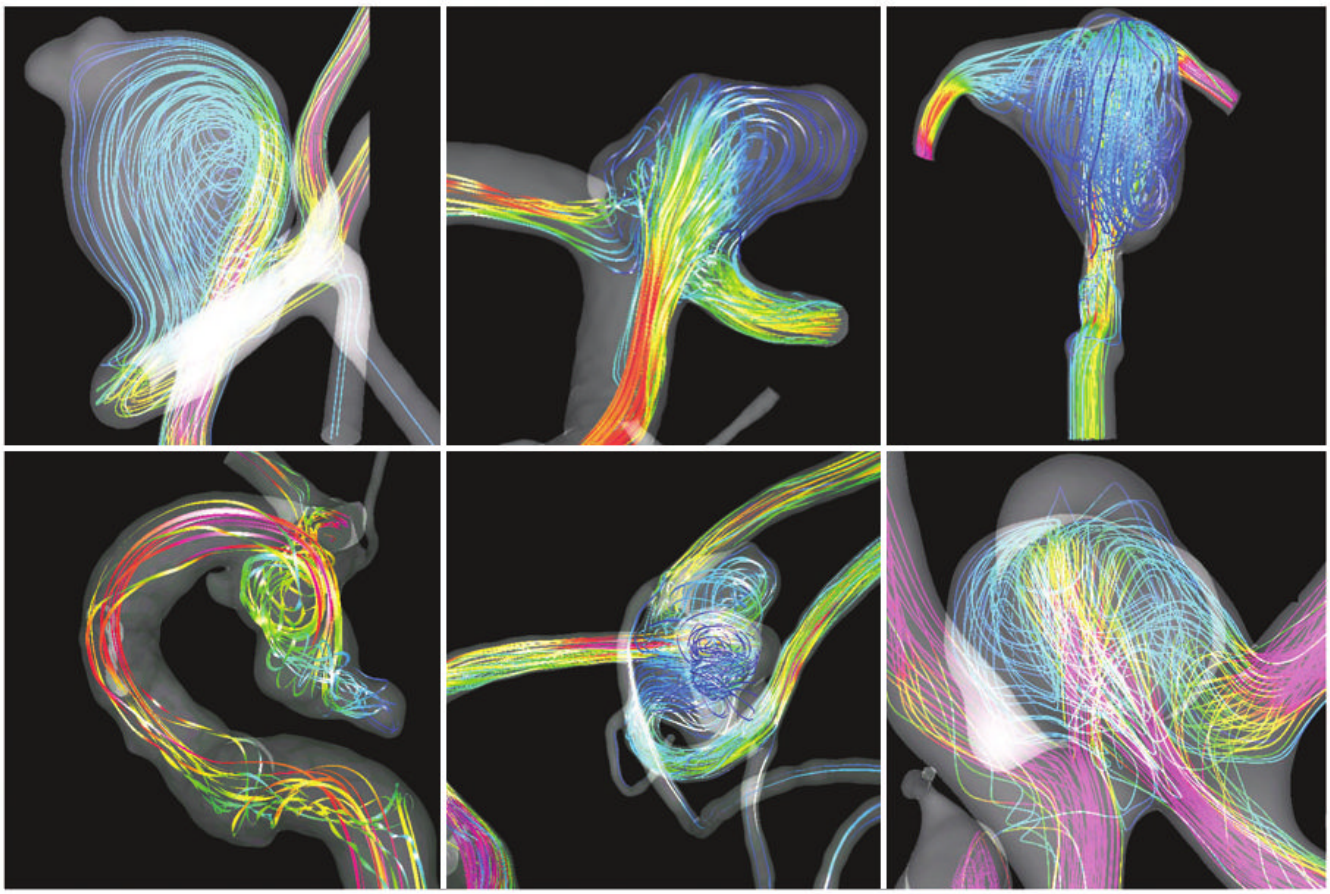

Figure 3.
Intra-aneurysmal flow patterns, ranging from simple patterns with a single recirculation region (*top left*) to complex patterns with several vortical structures that can be stable, moving, or intermittent during the cardiac cycle.

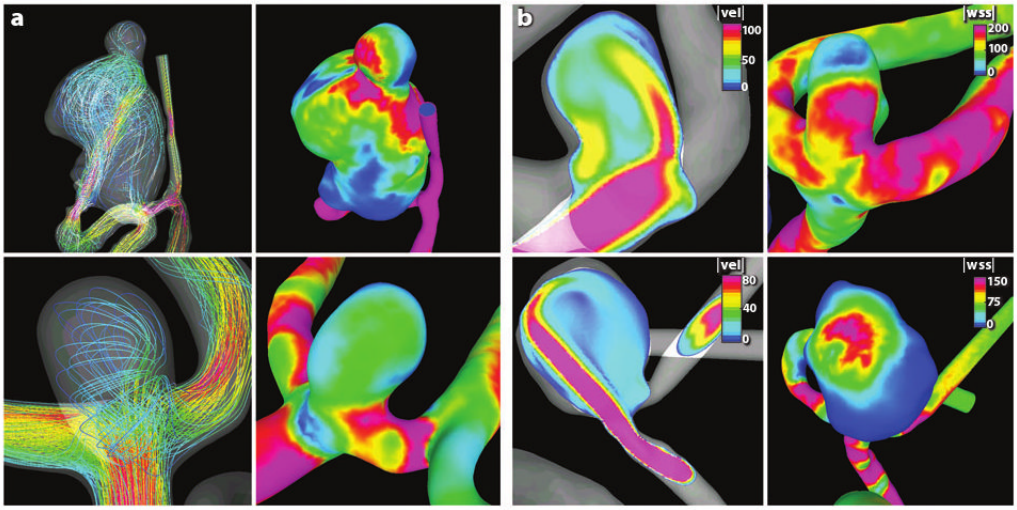

Figure 4.
(*a*) Aneurysms with concentrated inflow jet and regions of locally elevated wall shear stress (WSS) (*top panels*) and with diffuse inflow jet and WSS uniformly lower than the parent artery (*bottom panels*). (*b*) Aneurysms with large (*top panels*) and small (*bottom panels*) impingement regions compared to the aneurysm size.

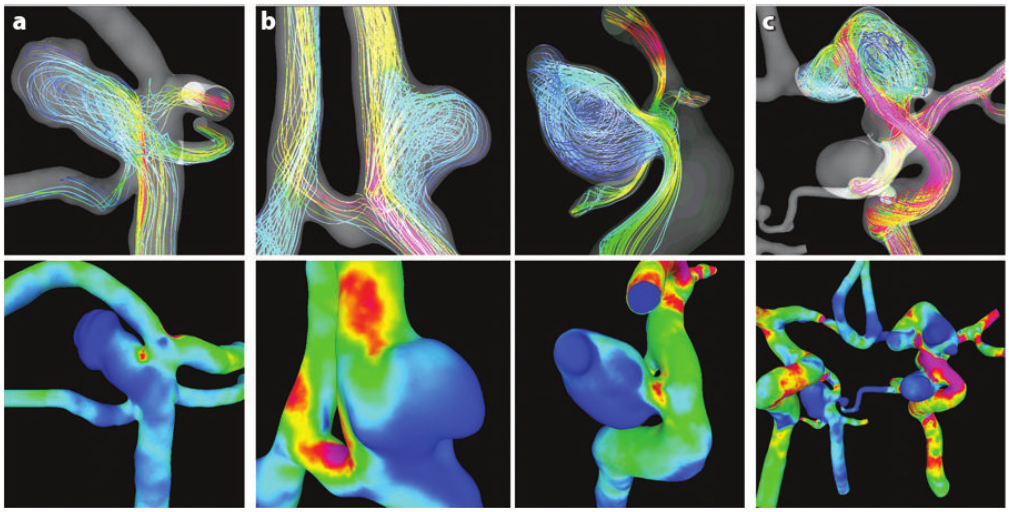

Figure 5.
Flow patterns (*top panels*) and wall shear stress distribution (*bottom panels*) of aneurysms with inflow regions located at the distal (*a*), side (*b*), and proximal (*c*) portions of the neck.

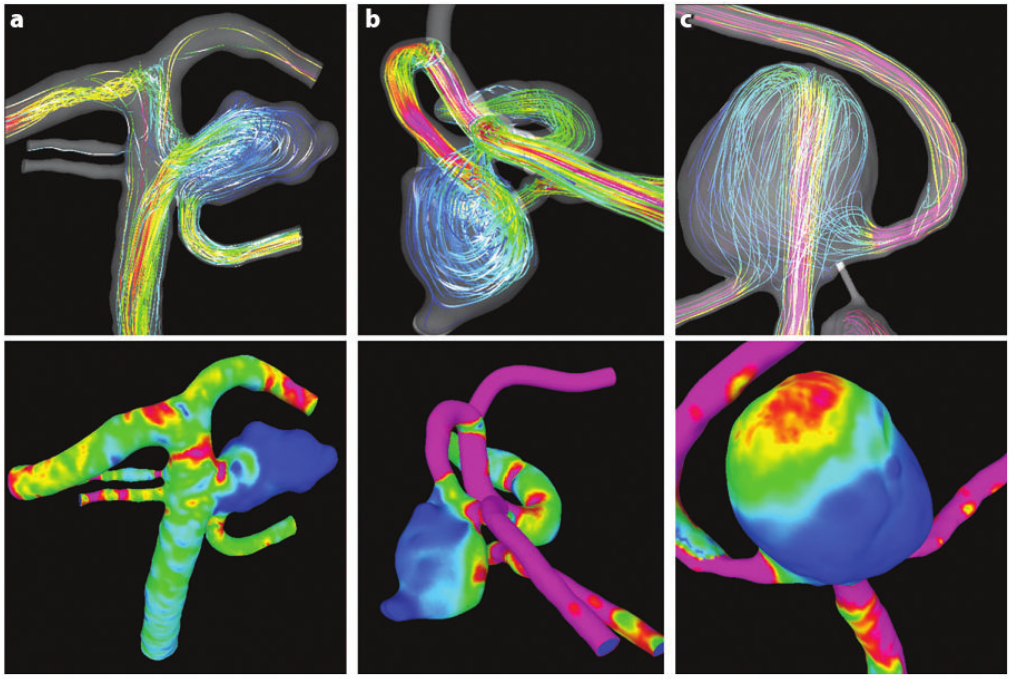

Figure 6.
Aneurysms with flow-impingement regions located at the neck (*a*), body (*b*) and dome (*c*) of the aneurysm. Flow patterns are shown in the top panels, and wall shear stress distribution is shown in the bottom panels.